Electronic Supplementary Information (ESI)

Octahedral distortion driven by $CsPbI_3$ nanocrystals reaction temperature – the effects on phase stability and beyond

Anastasia Matuhina[1], G. Krishnamurthy Grandhi[1], Maning Liu[1], Jan-Henrik Smått[2], N. S. M. Viswanath[3], Harri Ali-Löytty[4], Kimmo Lahtonen[5], Paola Vivo[1]**

[1]Hybrid Solar Cells, Faculty of Engineering and Natural Sciences, Tampere University, P.O. Box 541, FI-33014 Tampere University, Finland

[2]Laboratory of Molecular Science and Engineering, Åbo Akademi University, Henriksgatan 2, FI-20500 Turku, Finland

[3]School of Materials Science and Engineering, Chonnam National University, 77 Yongbong-ro, Buk-gu, Gwangju, 61186, Republic of Korea

[4]Surface Science Group, Faculty of Engineering and Natural Sciences, Tampere University, P.O. Box 692, FI-33014 Tampere University, Finland

[5]Faculty of Engineering and Natural Sciences, Tampere University, P.O. Box 692, FI-33014 Tampere University, Finland

Contents

1. Characterization

The X-ray photoelectron spectroscopy (XPS) measurements were conducted in an ultrahigh vacuum (UHV) system. The exposure to ambient air after PNC thin film fabrication was limited to 30 min before samples were loaded into the UHV. XPS data were measured using non-monochromatized Mg Ka X-rays (hν = 1253.6 eV) generated by a twin anode X-ray source (8025 Twin anode X-Ray source, V. G. Microtech) and a hemispherical electron spectrometer (CLAM4 MCD LNo5, V. G. Microtech). In order to mitigate possible X-ray damage, measurements were carried out using low X-ray power of 60 W (c.f. normal 300 W), high pass energy of 100 eV and total duration of X-ray exposure <15 min. Three consecutive sweeps of spectra were recorded and no change in chemical composition was observed during the data acquisition. The chemical states of the elements were determined from the XPS spectra by least-squares fitting of asymmetric Gaussian–Lorentzian lineshapes after subtracting a Shirley type background. The analysis was made in CasaXPS software version 2.3.17PR1.1[Fairley, N. CasaXPS: Spectrum Processing Software for XPS, AES and SIMS, Version 2.3.19PR1.0.; Casa Software Ltd.] using the Scofield photoionization cross-sections as relative sensitivity factors.[1] The binding energy scale was calibrated according to C 1s (C–C) set to 284.5 eV.

X-ray diffraction (XRD) patterns were recorded by Malvern Panalytical Empyrean Alpha 1 in a powder diffraction mode using Cu Kα radiation (λ = 1.5406 Å) and a cathode voltage and current of 45 kV and 40 mA, respectively. All the patterns were measured using identical settings (4–62° range, 0.0262° step size, and 17 s time per step). Samples were prepared by drop-casting from the as-synthesized dispersions on pre-cleaned microscopy cover glasses (20x20 mm). To ensure a proper comparison between the samples while guaranteeing a reasonable signal-to-noise ratio, a similar thickness was used for all samples. The structural information was derived from Rietveld refinement using the GSAS software suite.[2] A three-

dimensional visualization system for electronic and structural analysis (VESTA) was used to draw the crystal structures.[3] The phase purity of the as-synthesized samples was estimated via Rietveld refinement of the XRD results, considering full refinement of the crystallographic and instrumental parameters in the GSAS program suite. The distortion index values were extracted after completion of full patterned refinement process.

Transmission electron microscope (TEM) images were taken using JEM-F200 (200 kV). Carbon-coated Cu grids were dipped into the diluted NCs dispersions in hexane and dried in a vacuum desiccator (0.1 MPa) overnight before the measurement. Ultraviolet-visible (UV-vis) absorption spectra were recorded using a Shimadzu UV-3600 UV-vis-NIR spectrophotometer. Steady-state photoluminescence (PL) and absolute PL quantum yields (PLQYs) were measured using an FLS1000 spectrofluorometer (Edinburgh Instruments, UK) comprising a mountable integrating sphere. For all optical measurements, as-synthesized $CsPbI_3$ NCs dispersion (70 mg/mL) were further diluted in hexane with a dilution factor of 1:20 (NCs:hexane). The stability of the optical properties was monitored using the same diluted NCs dispersions. The time-resolved PL (TRPL) decays were recorded by using a time-correlated single-photon counting (TCSPC) apparatus equipped with a Picoharp 300 controller and a PDL 800-B driver for excitation and a Hamamatsu R3809U-50 microchannel plate photomultiplier for detection in 90° configuration. The instrument response time was 60 ps upon 405 nm excitation.

The current density (*J*)-voltage (*V*) characteristics were recorded with a Keithley 4250 source-monitor unit, under AM1.5G simulated sunlight (100 mW/cm^2 irradiance). The illumination was generated through an AAA- solar simulator (Sciencetech Inc.) and calibrated using a silicon reference cell. All samples in the form of films, solutions, and TEM specimens for stability studies were stored in dark under ambient conditions (RH~40%, 25°C). For the device stability study, all cells were stored in a dry box in dark (RH<10%, 25°C) and measured under ambient conditions.

2. Results

2.1 Surface analysis (XPS study)

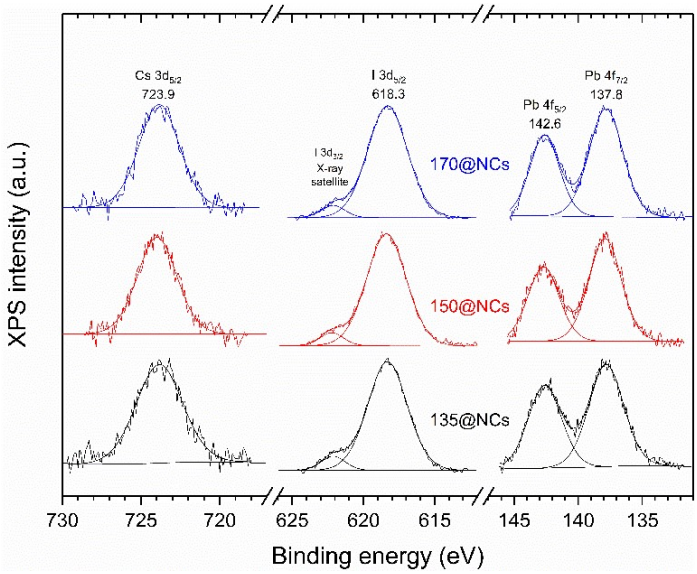

Figure S1. XPS spectra of Cs 3d5/2, I 3d5/2 and Pb 4f measured for 135@NCs, 150@NCs, and 170@NCs thin film samples in their as-synthesized condition.

To avoid the formation of Pb^0 upon the typical high pass energy of 10-20 eV during the XPS measurements,[4] a stronger high pass energy of 100 eV was applied to secure low X-ray exposure, therefore, to mitigate possible X-ray damage.

2.2 Structural analysis

Table S1. Lattice parameters and residual fitting parameters of γ-$CsPbI_3$ NCs, which are obtained by performing Rietveld refinement on X-ray diffraction data obtained at room temperature. The numbers in parentheses are the estimated standard deviations of the last significant figure.

Sample	Space group	a (Å)	b (Å)	c (Å)	V (Å)^3	Z	$^aR_{wp}$ (%)	$^b\chi^2$	^{c}D
γ-$CsPbI_3$ (135 °C)	*P n a m*	9.14(4)	8.48(3)	12.49(6)	971(5)	4	2.5	1.4	8.0%
γ-$CsPbI_3$ (150 °C)	*P n a m*	9.14(4)	8.38(3)	12.38(6)	962(3)	4	2.8	1.3	1.3%

γ-$CsPbI_3$ (170 °C)	*P n a m*	9.14(4)	8.27(3)	12.35(6)	956(12)	4	2.2	1.2	3.8%

[a]Residual weighing factor [b]goodness of fit [c]distortion index value

Table S2. Refined structural parameters of orthorhombic γ-$CsPbI_3$ NCs, which are obtained from X-ray diffraction data at room temperature. The numbers in parentheses are the estimated standard deviations of the last significant figure.

Atom	Wyckoff position	*x*	*y*	*z*	$100xU_{iso}(Å)^2$
Cs	4*c*	0.4599(1)	0.5050(7)	0.2500(3)	0.0126(7)
Pb	4*b*	0.0000(0)	0.5000(0)	0.0000(0)	0.0126(0)
I	4*c*	0.0011(3)	0.6244(2)	0.2500(7)	0.2322(5)
I	8*d*	0.3225(7)	0.6304(3)	-0.0312(5)	0.0440(3)

2.3 Optical stability study

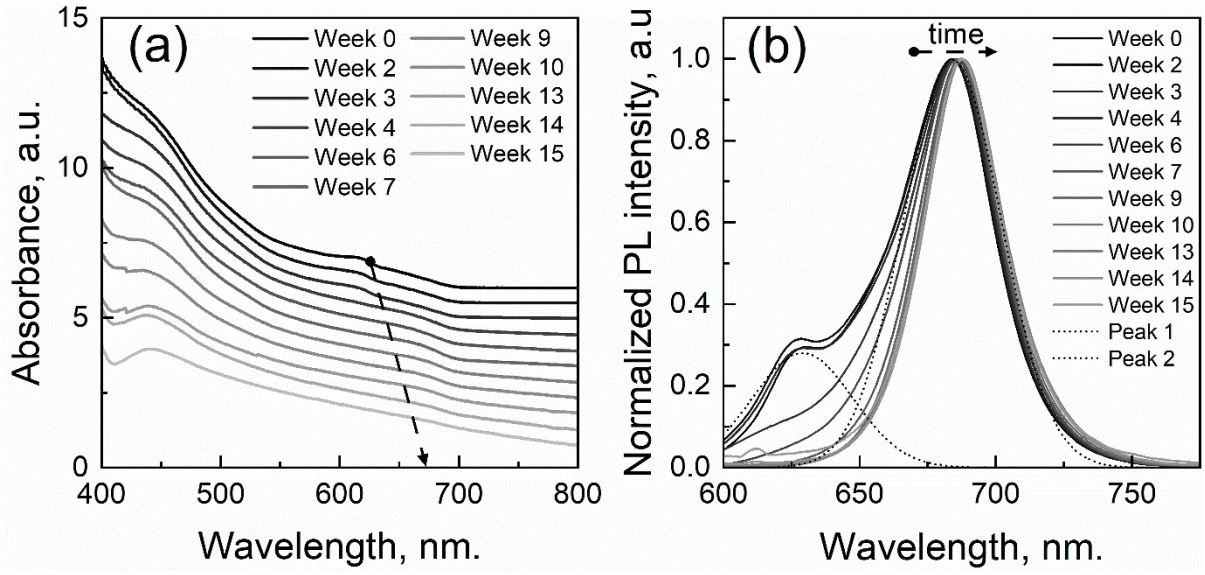

Figure S2. Optical stability of $CsPbI_3$ NCs dispersion synthesized at 135 °C under ambient conditions: (a) UV-Vis absorption spectra and (b) Normalized PL spectra of the NCs. The dot lines are deconvoluted first PL spectrum with two Gaussian peaks centered at 629 and 684 nm for the determination of respective FWHM.

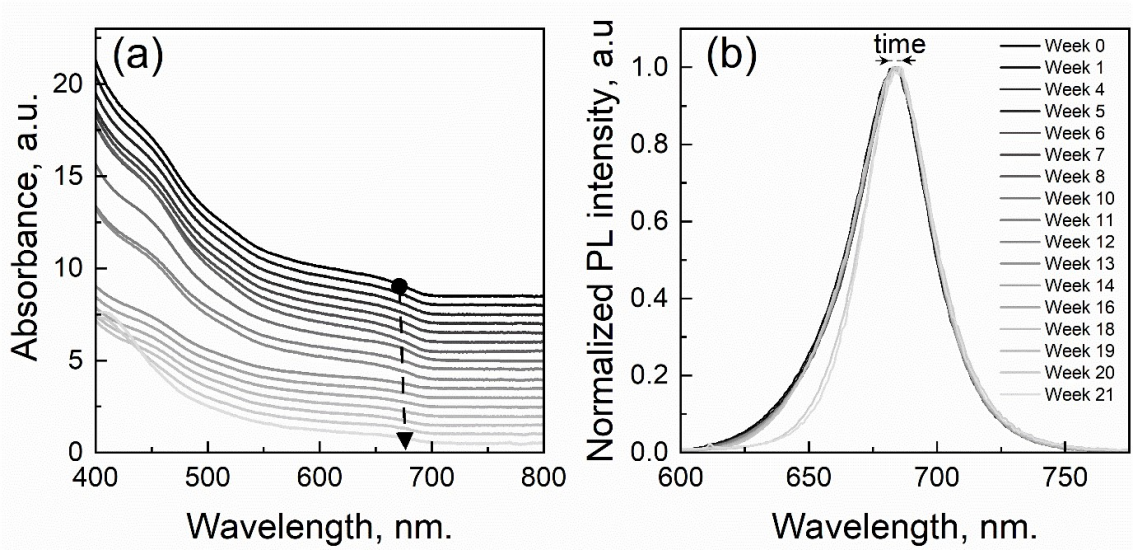

Figure S3. Optical stability of $CsPbI_3$ NCs dispersion synthesized at 150°C under ambient conditions: (a) UV-Vis absorption spectra and (b) Normalized PL spectra of the NCs.

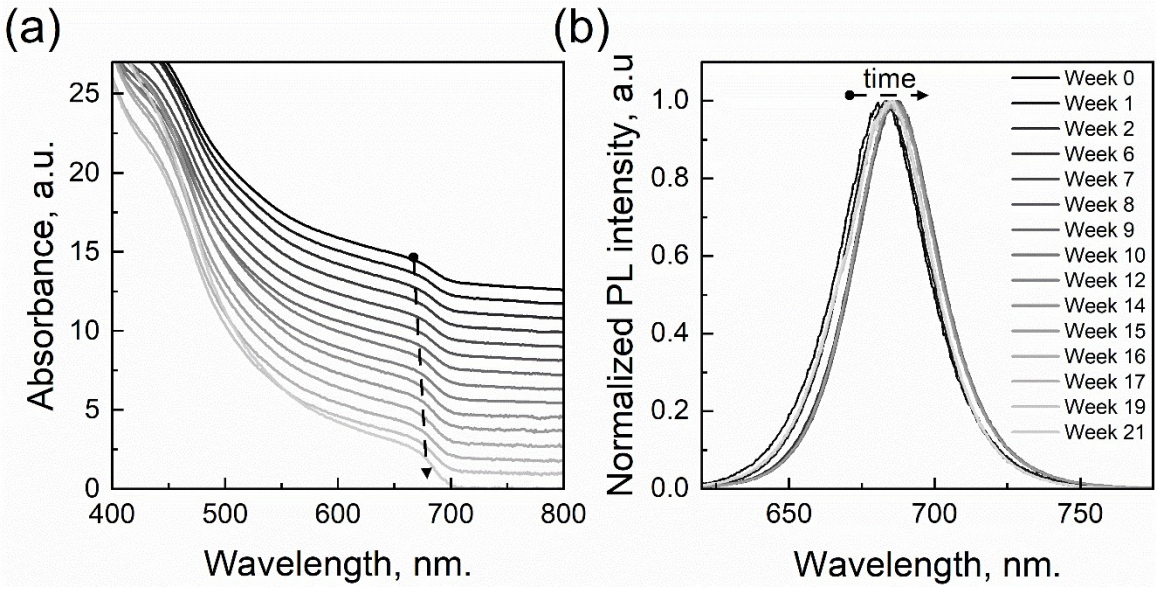

Figure S4. Optical stability of $CsPbI_3$ NCs dispersion synthesized at 170 °C under ambient conditions: (a) UV-Vis absorption spectra and (b) Normalized PL spectra of the NCs.

We attribute the longer stability of our NC dispersions, even for the case of commonly reported 170 °C[5] injection temperature (Figure S4), to the modification of the NC purification protocol. The introduction of a polar solvent during the purification step could potentially damage the NC surface, in turn enabling an easier moisture penetration. Therefore, our NCs

with unaltered surface exhibit higher stability compared to the reported ones. To confirm this point, MeOAc purification was also tested for comparison, as discussed in detail in the Experimental Section in main content.

2.4 Photophysical study

Table S3. Summary of TRPL data for $CsPbI_3$ NCs (synthesized at different temperatures), as obtained from the bi-exponential fitting of TRPL decays. The τ_1, A_1 (%) and τ_2, A_2 (%) are lifetime and contribution factor of the non-radiative and radiative components of the PL decays, respectively.

Sample	A_1 (%)	τ_1 (ns)	A_2 (%)	τ_2 (ns)
135@NCs	64.0	19.1	36.0	58.2
150@NCs	63.7	23.0	36.3	50.1
170@NCs	56.0	18.5	44.0	47.0

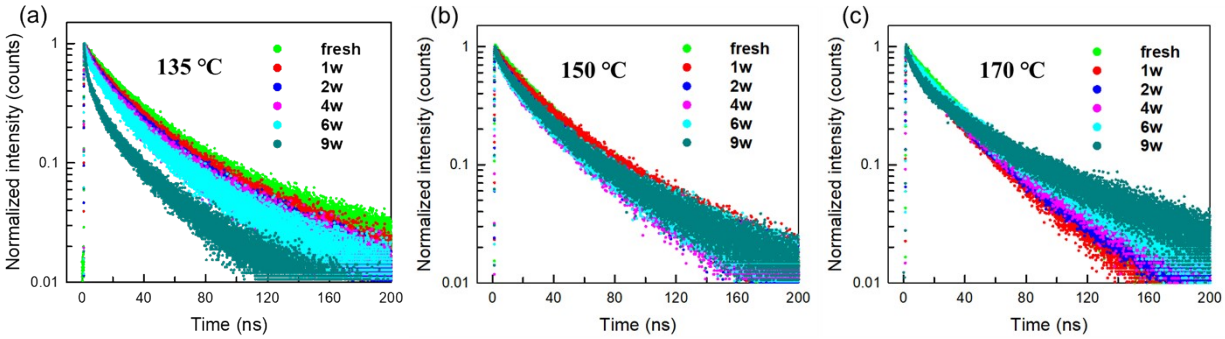

Figure S5. Storage time (w = weeks) dependent TRPL decays of $CsPbI_3$ NCs formed at the targeted injection temperatures: (a) 135 °C, (b) 150 °C, and (c) 170 °C. The NC dispersions were stored in dark under ambient conditions (RH~40%, T=25 °C).

2.5 Photostability testing

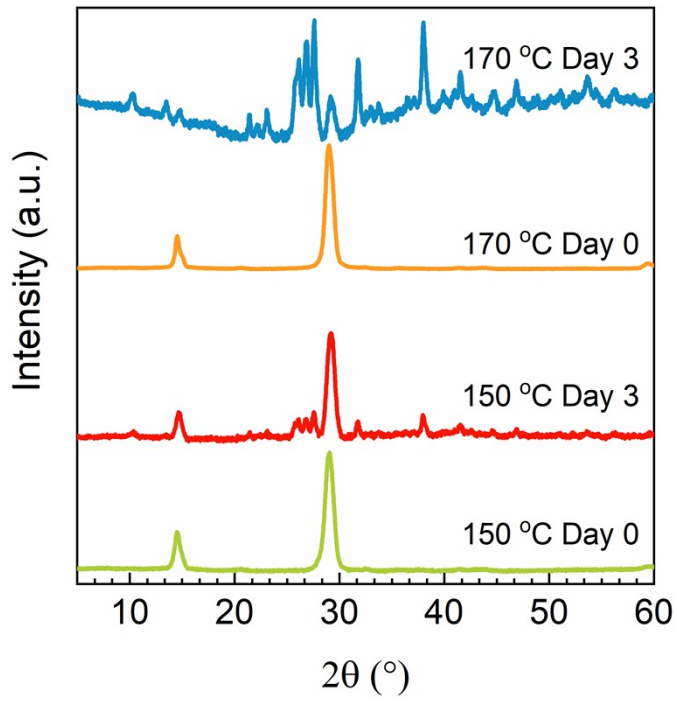

Figure S6. Storage time-dependent XRD patterns of $CsPbI_3$ NC films synthesized at 150 °C and 170 °C under continuous light illumination (1460 lux). 150@NCs still mainly preserve the black phase after 3 days of light exposure, while 170@NCs transform to the yellow phase within the same time frame.

2.6 Distortion index analysis

Typically, the distortion index value of a selected polyhedron is determined by two parameters. The first one is cation and anion disorder around the polyhedron, and the second one is its average bond distance. Hence, firstly, we determined the cation disorder of Pb and the anion disorder of I by calculating the U_{iso}, which is the positional disorder parameter of the cation and anion.[6,7] **Figure S6**a-c demonstrates, among the three samples, that135@NCs sample exhibits a higher cation and anion disorder around the PbI_6 octahedra and, hence, a higher distortion index value. Secondly, we also calculated the average Pb-I bond distance of the as-synthesized samples. The 135@NCs sample shows a larger average bond distance than the other samples (Figure S6d). Therefore, a higher cation and anion disorder and a larger Pb-I bond length of Pb-I octahedra lead to a high distortion index value for 135@NCs.

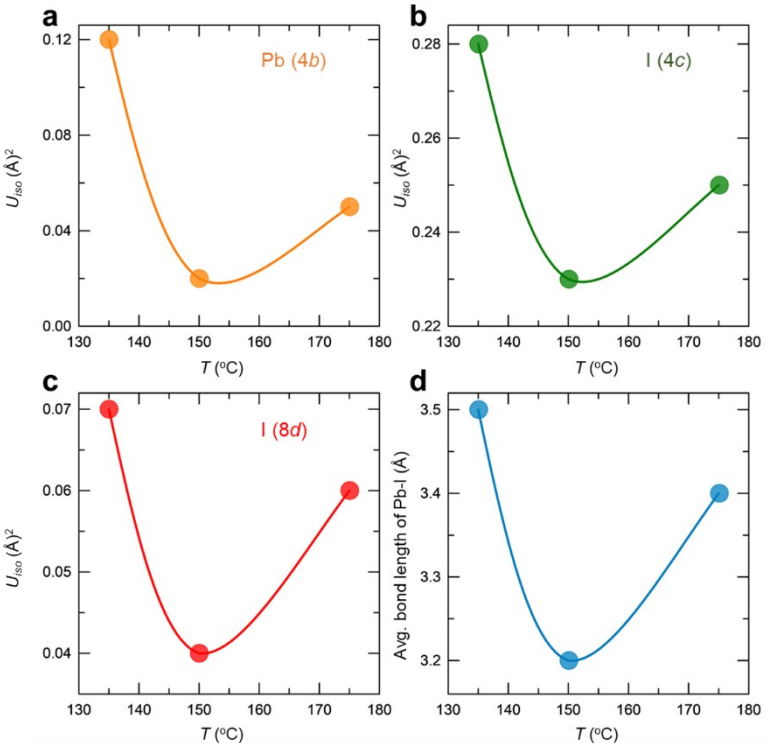

Figure S7. The variation of injection temperature *vs.* U_{iso} for (a) Pb atom and (b) and (c) for I atoms. (d) The average Pb-I bond distance as a function of the injection temperature.

2.7 Morphological stability study

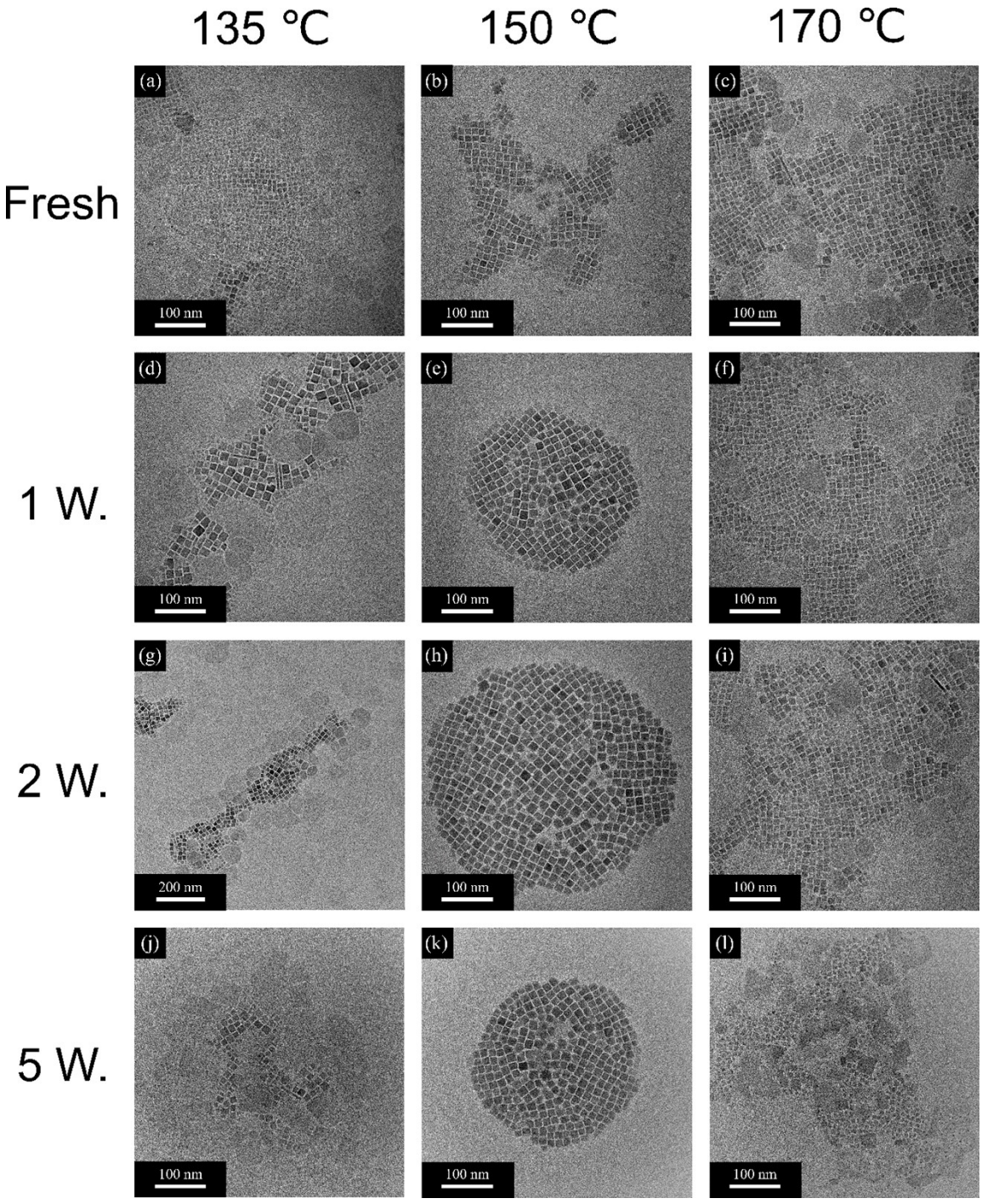

Figure S8. TEM images of 135@NCs (a, d, g, j), 150@NCs (b, e, h, k), and 170@NCs (c, f, i, l), measured in week (W) 0, 1, 2, and 5 of storage under ambient conditions, respectively.

2.8 Performance of $CsPbI_3$ NCs-based solar cells

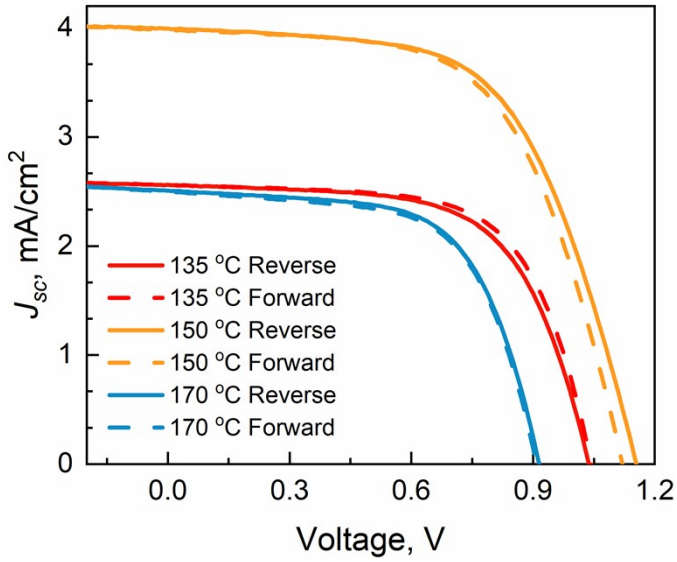

Figure S9. *J–V* curves of best 135-170@NCs-based solar cells under 1 sun illumination (100 mW/cm^2). The scan rate is 50 mV/s.

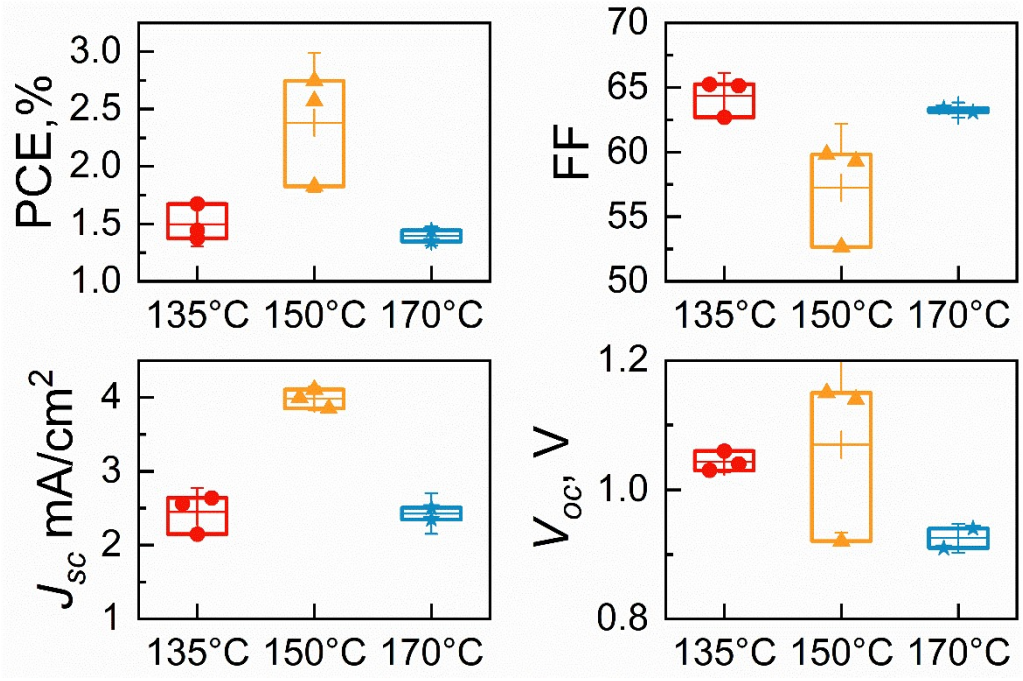

Figure S10. Photovoltaic parameters of *n-i-p* devices with structure of FTO/c-TiO_2/$CsPbI_3$ NCs/spiro-OMeTAD/Au, for 120@NCs, 135@NCs, 150@NCs, and 170@NCs, respectively.

Table S4. Storage time dependent photovoltaic parameters for $CsPbI_3$ NCs-based solar cells with different injection temperatures.

Sample	Day 0				Day 4				Day 18				Day 26			
	J_{sc}, mA/cm^2	V_{oc}, V	*FF*	PCE, %	J_{sc}, mA/cm^2	V_{oc}, V	*FF*	PCE, %	J_{sc}, mA/cm^2	V_{oc}, V	*FF*	PCE, %	J_{sc}, mA/cm^2	V_{oc}, V	*FF*	PCE, %
135@NCs	2.6	1.0	63.5	1.7	1.9	1.0	63.9	1.3	2.4	1.1	61.8	1.6	2.1	1.0	60.9	1.2
150@NCs	4.0	1.2	59.8	2.8	3.9	1.1	68.7	**3.0**	3.5	1.1	65.0	2.6	3.6	1.1	67.2	2.7
170@NCs	2.5	0.9	63.3	1.4	0.6	0.8	33.0	0.1	1.2	0.9	57.4	0.6	0.8	0.9	58.5	0.4

References

1 J. H. Scofield, *J. Electron Spectros. Relat. Phenomena*, 1976, **8**, 129–137.

2 B. H. Toby, *J. Appl. Crystallogr.*, 2001, **34**, 210–213.

3 K. Momma and F. Izumi, *J. Appl. Crystallogr.*, 2011, **44**, 1272–1276.

4 J. D. McGettrick, K. Hooper, A. Pockett, J. Baker, J. Troughton, M. Carnie and T. Watson, *Mater. Lett.*, 2019, **251**, 98–101.

5 J. Shamsi, A. S. Urban, M. Imran, L. De Trizio and L. Manna, *Chem. Rev.*, 2019, **119**, 3296–3348.

6 R. E. Dinnebier, A. Leineweber, J. S. O. Evans, R. E. Dinnebier, A. Leineweber and J. S. O. Evans, *Rietveld refinement*, De Gruyter, 2018.

7 M. Yashima and T. Takizawa, *J. Phys. Chem. C*, 2010, **114**, 2385–2392.